Supplementary Information (SI) for Inorganic Chemistry Frontiers.
This journal is © the Partner Organisations 2025

Real-Time Vibrational Fingerprinting of Liquid-Phase Sulfide Electrolyte Synthesis via In Situ Raman Spectroscopy

Zachary Warren[1,2], Thomas Poupeau[3], Beyza Batu[4], Nataly Carolina Rosero-Navarro[1*]

[1]Instituto de Cerámica y Vidrio– CSIC, C/Kelsen 5, Madrid, Spain, 28049

[2]Universidad Autónoma de Madrid, Ciudad Universitaria de Cantoblanco, 28049 Madrid, Spain

[3]Département Matériaux – Campus de Luminy 163 avenue de Luminy, case 925 13288 Marseille Cedex 09, France

[4]Sakarya University, Department of Metallurgical & Materials Engineering, Esentepe Campus, 54050, Sakarya, Türkiye

Supporting Information

Contents

Introduction

This Supporting Information provides additional figures, calibration data, kinetic analyses, and statistical evaluations that complement the main manuscript. These materials supply further validation of the experimental setup, illustrate the reproducibility of kinetic measurements, and expand upon the thermodynamic analyses described in the main text.

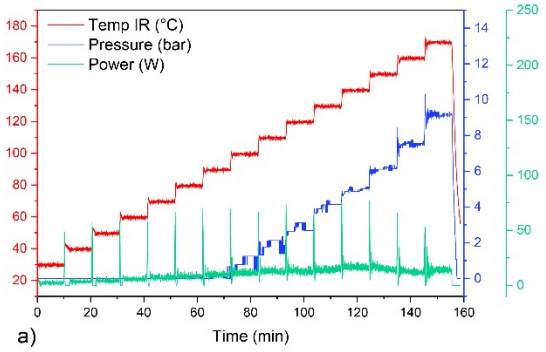

Figure S1. Microwave assisted heating of P_4S_{10} in acetonitrile

Figure S1 shows the reaction profile of P_4S_{10} heated at 10 °C increments while measuring the reaction vessel pressure (blue) in bar, the power input (green) by the reactor in Watts, and the temperature (red) in degrees Celsius. The significant change in pressure observed at approximately 70 mins corresponds to the temperature of 90 °C. At temperatures above 82 °C, the acetonitrile is predominantly in the gas phase, thus exhibiting higher pressure on the reaction system.

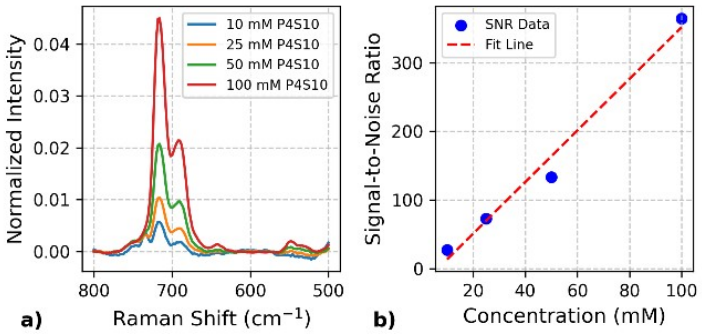

Figure S2. Calibration and Analytical Benchmarks

Figure S2 shows (a) the Raman spectra for standards of P_4S_{10} in acetonitrile (ACN) under reaction conditions and (b) the calibration curve of signal-to-noise ratio (SNR) versus concentration. This calibration established the analytical performance of the Raman setup, yielding a limit of detection (LOD) of 0.78 mM and a limit of quantification (LOQ) of 2.60 mM for the P=S stretching vibration at ~716 cm^{-1}. These benchmarks ensure reliable quantification of spectral changes during kinetic monitoring and confirm the sensitivity of the in situ Raman configuration.

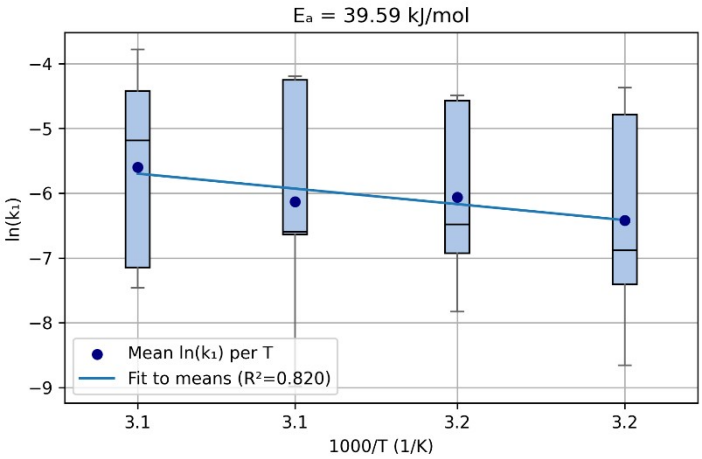

Figure S3. Arrhenius Analysis

Figure S3 presents the Arrhenius plot derived from temperature-dependent rate constants of the initial reaction step. A linear fit of ln(k) versus 1000/T provided the activation energy (E_a(mw) = 39.59 kJ mol^{-1}) and corresponding pre-exponential factor. These parameters highlight the relatively low energetic barrier associated with microwave-assisted synthesis, consistent with the accelerated nucleation and growth processes observed in the real-time Raman data.

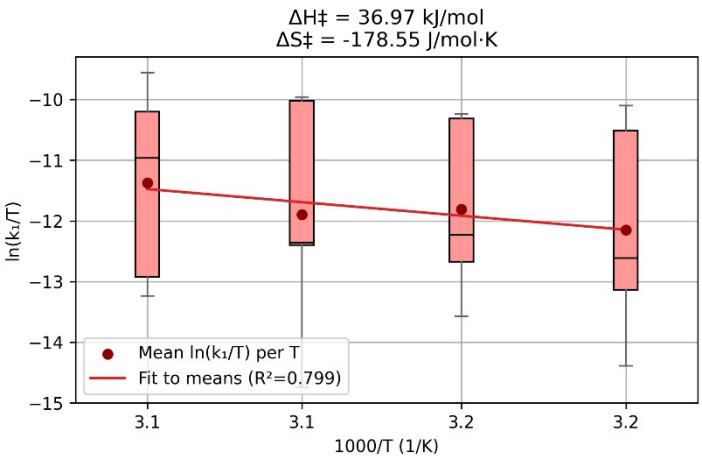

Figure S4. Eyring Analysis

Figure S4 displays the Eyring plot, where ln(k/T) is plotted against 1000/T. From the slope and intercept, the enthalpy (ΔH‡ = 36.97 kJ mol^{-1}) and entropy (ΔS‡ = −178.55 J $mol^{-1} \cdot K^{-1}$) of activation were extracted. The modest enthalpy requirement and strongly negative entropy indicate an energetically accessible yet ordered transition state, reflecting precursor alignment and restructuring during the early stages of thiophosphate formation.

Parameter	Value	Units
Activation Energy (Ea)	39.59271364	kJ/mol
Arrhenius slope	-4762.17388	(ln k)·K
Arrhenius intercept	9.038907003	ln k
Arrhenius R^2	0.819586792	-
Enthalpy of Activation (ΔH‡)	36.96956295	kJ/mol
Entropy of Activation (ΔS‡)	-178.5466277	J/mol·K
Eyring slope	-4446.663814	(ln k/T)·K
Eyring intercept	2.284559513	ln k/T
Eyring R^2	0.798537062	-

Table S1. Fit Parameters for Arrhenius and Eyring Analysis

Table S1 summarizes the linear regression outputs for both Arrhenius and Eyring fits, including slopes, intercepts, coefficients of determination (R^2), and the derived thermodynamic parameters. These values provide the quantitative basis for the kinetic and thermodynamic discussion presented in the manuscript.

Tables S2–S4. Statistical Analysis of Kinetic Parameters

To assess reproducibility and temperature dependence, statistical analyses of the kinetic parameters (k_1, k_2, and maximum slope) are provided in Tables S2–S4. Each table reports the mean, standard deviation, quartiles, interquartile range (IQR), and standard error of the mean (SEM) for five independent trials at each temperature.

Temp	count	mean	std	min	median	max	q25	q75	IQR	sem
30	5	0.006128	0.003783	0.00132	0.006849	0.010431	0.003275	0.008763	0.005488	0.001692
35	5	0.004556	0.005629	0.000174	0.001023	0.012624	0.000608	0.00835	0.007742	0.002518
40	5	0.004892	0.005393	0.000399	0.001529	0.011184	0.000981	0.010366	0.009385	0.002412
45	5	0.006412	0.007523	0.000126	0.001366	0.015061	0.001312	0.014196	0.012884	0.003364
50	5	0.008363	0.009332	0.000576	0.005605	0.022835	0.00079	0.012009	0.011219	0.004173

Table S2: Statistical analysis of k_1 values across temperatures, illustrating consistent temperature dependence of the nucleation rate constant.

Temp	count	mean	std	min	median	max	q25	q75	IQR	sem
30	5	1.79E-05	2.5E-05	4.06E-20	1.6E-16	5.2E-05	6.92E-18	3.73E-05	3.73E-05	1.12E-05
35	5	6.25E-05	6E-05	1.98E-19	8.05E-05	0.000132	5.4E-19	1E-04	1E-04	2.68E-05
40	5	5.94E-05	5.53E-05	2.77E-21	8.43E-05	0.000115	3.62E-18	9.72E-05	9.72E-05	2.47E-05
45	5	6.9E-05	6.54E-05	5.72E-17	9.81E-05	0.000144	8.44E-16	0.000103	0.000103	2.93E-05
50	5	8.26E-05	7.66E-05	4.36E-24	0.000118	0.000157	6.92E-17	0.000138	0.000138	3.43E-05

Table S3: Statistical analysis of k_2 values, reflecting the autocatalytic growth contribution and its increase with temperature.

Temp	count	mean	std	min	median	max	q25	q75	IQR	sem
30	5	0.589532	0.3339	0.195824	0.630752	0.977258	0.30895	0.834874	0.525923	0.149324
35	5	0.543824	0.41212	0.223984	0.303279	1.194549	0.284542	0.712764	0.428222	0.184306
40	5	0.567042	0.385587	0.249546	0.323129	1.016964	0.286802	0.958767	0.671965	0.17244
45	5	0.748759	0.576058	0.311148	0.356523	1.431228	0.319758	1.325137	1.005379	0.257621
50	5	0.938988	0.753321	0.365142	0.612345	2.168254	0.40797	1.141228	0.733259	0.336896

Table S4: Statistical analysis of maximum slope values, representing the steepest point of the reaction curve and providing an additional descriptor of kinetic acceleration.

The Arrhenius and Eyring analyses across temperatures (Figures S2 and S3) exhibit statistical variability between trials, as reflected by the relatively high standard error of the mean (SEM) compared to the mean values reported in Tables S2–S4. This variability is attributed to particle–surface interactions during the $Li_2S + P_4S_{10}$ reaction: differences in precursor particle size and morphology can influence the degree of contact, dissolution, and subsequent reactivity, thereby introducing scatter into the kinetic data. Additionally, the number of replicates performed at each temperature (five trials) provides a reliable but limited statistical sample, which naturally constrains the precision of calculated parameters. Despite these factors, the datasets consistently display an upward trend across temperature, enabling estimation of activation energy and thermodynamic parameters. These observations emphasize the importance of reporting full statistical descriptors alongside mean values, ensuring transparency and reproducibility in the kinetic analysis.

Late-Stage Reaction Raman Spectra

To better understand the evolution of PS_4^{-3} in acetonitrile, the reactions $3Li_2S$-$0.5P_4S_{10}$ and $5Li_2S$-$0.5P_4S_{10}$-2LiCl were monitored with *in situ* Raman spectroscopy and are illustrated below in figures S5 and S6, respectively.

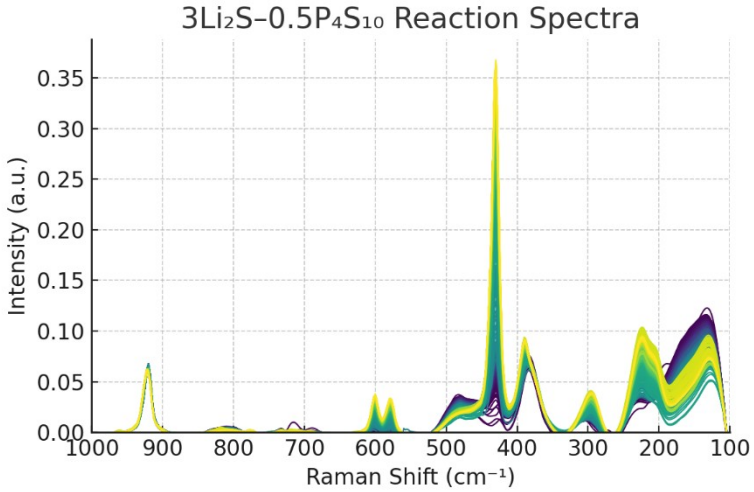

Figure S5. The Raman spectra of 24 hr of reaction time for the reaction $3Li_2S$-$0.5P_4S_{10}$ in acetonitrile.

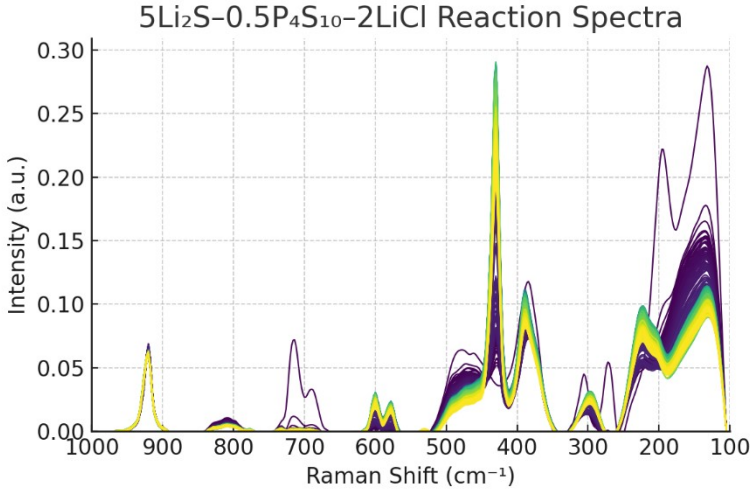

Figure 6S. The Raman spectra of 24 hr of reaction time for the reaction $5Li_2S$-$0.5P_4S_{10}$-2LiCl in acetonitrile.

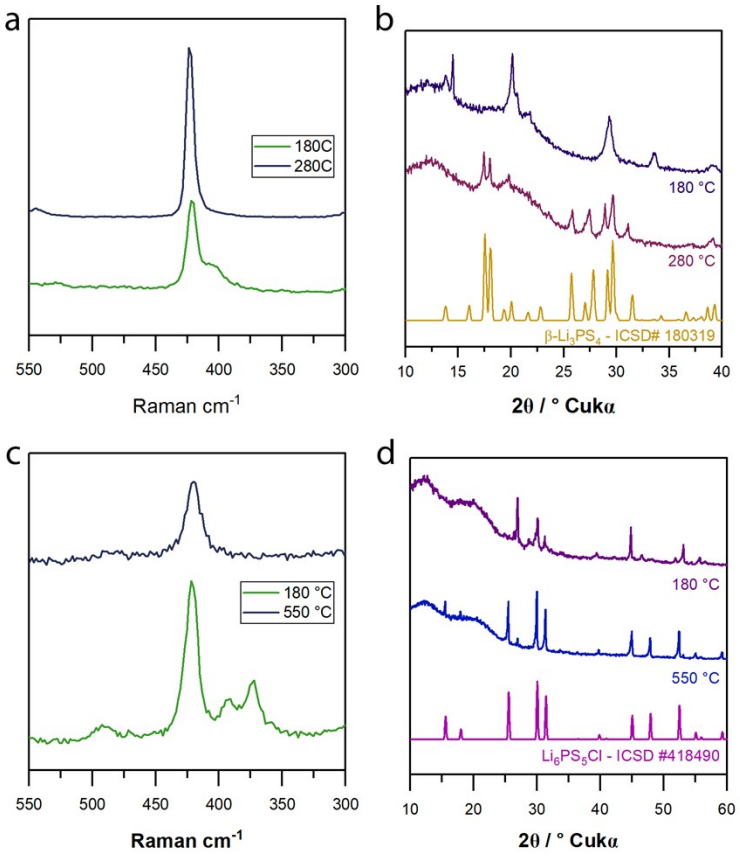

Figure S7. The dried and heat-treated phases of the sulfide solid electrolytes synthesized during the in situ synthesis in Figure 6. a) The Raman shift and b) XRD patterns of the LPS electrolyte after 180 and 280 °C. c) The Raman shift and d) XRD patterns of the LPSC electrolyte after 180 and 550 °C.

Summary of Supporting Information

The data provided in this Supporting Information confirm the reliability and reproducibility of the *in situ* Raman–kinetic framework used in the main study. Calibration of detection limits, derivation of Arrhenius and Eyring parameters, and statistical evaluation of trial replicates collectively support the mechanistic interpretation of thiophosphate formation. These complementary materials establish a solid foundation for extending the methodology to other stoichiometries, solvents, and related solid electrolyte systems.